

# Double-relativistic-electron-shell laser proton acceleration

Yongsheng Huang,\* Naiyan Wang, Xiuzhang Tang, and Yijin Shi

*China Institute of Atomic Energy, Beijing 102413, China.*

Yan Xueqing

*Institute of Heavy Ion Physics, Peking University, Beijing 100871, China*

Zhang Shan

*Beijing Normal University, Beijing 100875, China*

(Dated: November 10, 2018)

## Abstract

A new laser-proton acceleration structure combined by two relativistic electron shells, a suprathreshold electron shell and a thermal electron cloud is proposed for  $a \gtrsim 80\sigma_0$ , where  $a$  is the normalized laser field and  $\sigma_0$  is the normalized plasma surface density. In the new region, a uniform energy distribution of several GeV and a monoenergetic hundreds-of-MeV proton beam have been obtained for  $a = 39.5$ . The first relativistic electron shell maintains opaque for incident laser pulse in the whole process. A monoenergetic electron beam has been generated with energy hundreds of MeV and charge of hundreds of pC. It is proposed a stirring solution for relativistic laser-particle acceleration.

Laser-ion acceleration has been an international research focus[1–3], however it is still a challenge to obtain mono-energetic proton beams larger than 100MeV. Although the field in the laser-plasma acceleration is three to four orders higher than that of the classic accelerators, it decreases to zero quickly in several pulse durations for target normal sheath acceleration (TNSA)[2] for  $a \ll \sigma_0 = \frac{n_e l_e}{n_c \lambda}$ , where  $a = eE_l/m\omega c$ ,  $E_l$  is the electric field of the laser pulse,  $\omega$  is the laser frequency,  $e$  is the elementary charge,  $m$  is the electron mass,  $c$  is the light velocity,  $n_0$  is the initial plasma density,  $n_c$  is the critical density,  $\lambda$  is the wave length,  $n_e$  is the electron density,  $l_e$  is the thickness of the electron shell. As a promising method to generate relativistic mono-energetic protons, radiation pressure acceleration (RPA) has attracted more attention[3, 4, 6, 7] and becomes dominant in the interaction of the ultra-intense laser pulse with thin foils if  $a \approx \sigma_0$ . Even in the unlimited ion acceleration[7], only the ions trapped in the electron shell can obtain efficient acceleration, therefore, the total charge of the ion beam is quite limited due to the transverse expansion[7]. Although in RPA region, the energy dispersion will become worse with time.

Fortunately, for  $a \gtrsim 80\sigma_0$ , in the relativistic case, a new acceleration region appears: double relativistic electron shells come into being. The ions between the two electron shells will be accelerated most efficiently and obtain a uniform energy distribution. The first electron shell is ultra-relativistic and is totally separated from the ions. The second electron shell comes into being in the potential well induced by the electron recirculation and will also be relativistic. It is in the ion region and follows the ion front and forms a potential well which traps energetic ions and accelerates them to be quasi-mono-energetic and relativistic. Following the second electron shell, a suprathermal electron beam comes into being and induces another potential well which can also trap lots of ions and accelerate them to obtain a monoenergetic relativistic one. On the whole, the maximum ion energy can reach several GeV and a relativistic monoenergetic ion beam with relative energy dispersion smaller than 5% can be obtained.

As a ultraintense laser pulse is shot on a ultra-thin plasma foil for  $a \gtrsim 80\sigma_0$ , the electron shell is compressed to ultra-high density and pushed forward to be separated from the ion shell totally, and gains ultra-relativistic energy that can make sure it opaque for the laser pulse. In the whole process, the first electron shell keeps opaque for the incident laser pulse and is pushed by it continuously. According to Eq. (22)[7], it can be satisfied that the

opaqueness condition of electron shell for laser in the acceleration:

$$a_0 \leq \pi(\gamma_e + p_e)\hat{n}_e\hat{l}_e, \quad (1)$$

since  $d \ln(p\hat{n}_e\hat{l}_e)/dt > 0$ , as pointed by Bulanov,  $p \propto t^{1/3}$  is the normalized electron momentum, and  $n_e l_e = n_0 l_0$  in the no transverse expansion case, where the electron density  $n_e, n_0$  are normalized by  $n_c$  and  $l_e$  is normalized by  $\lambda$ ,  $a_0 = eE_0/m\omega_0 c$ ,  $E_0$  is the electric field of the laser pulse,  $\omega_0$  is the laser frequency,  $e$  is the elementary charge,  $m$  is the electron mass,  $c$  is the light velocity,  $n_0$  is the initial plasma density,  $n_c$  is the critical density,  $\lambda$  is the wave length. In the ultra-relativistic case, the r.h.s. of Eq. (1) is approximate  $2\pi p\hat{n}_e\hat{l}_e$ .

For  $a = 39.5$  and  $\hat{n}_e\hat{l}_e = 49 \times 0.01 = 0.49$ ,  $a \approx 81\hat{n}_e\hat{l}_e$ . When the laser pulse interacts with the plasma shell, the electrons are compressed to high density and pushed forward to be separated from the ion shell. As shown by Figure 1 (c) and (d), at  $t = 25\text{fs}$ , the normalized momentum of the electron shell reaches 20–100. With Eq. (1), the compressed high-density electron shell is opaque for the laser pulse as shown by Figure 1 (f). The electrons will be accelerated efficiently and continuously by the radiation pressure of the laser.

This high-density relativistic electron shell is called the first relativistic electron shell. Between the first electron shell and the ions, a uniform space-charge separation field forms and accelerates the ions at the ion front and drags the electrons as shown by Figure 1 (e). The "capacity" field is decided by the surface density of the electron shell:

$$E_{cap} = \frac{en_e l_e}{\epsilon_0}, \quad (2)$$

For  $n_e = 5.5 \times 10^{22}/\text{cm}^3$ ,  $l_e = 10\text{nm}$ , the stable field is  $9.95 \times 10^{12}\text{V/m}$ , which accelerates the ions at the rear of the ion shell continuously. Therefore the maximum ion energy is proportional to the acceleration length,  $d_{acc}$ ,

$$E_i = E_{cap}d_{acc}(\text{eV}), \quad (3)$$

before the electron shell breaks up.

After several hundreds of femtoseconds, some electrons leak out from the electron shell continuously and move backward and round again and follow the ion front, however, they can not catch the ion front. Figure 2 (c), (e) and (f) shows the electron recirculation, the decrease of the separation field, and the formation of the potential well for electrons at  $t = 450\text{fs}$  respectively. The normalized maximum electron momentum reaches about 500

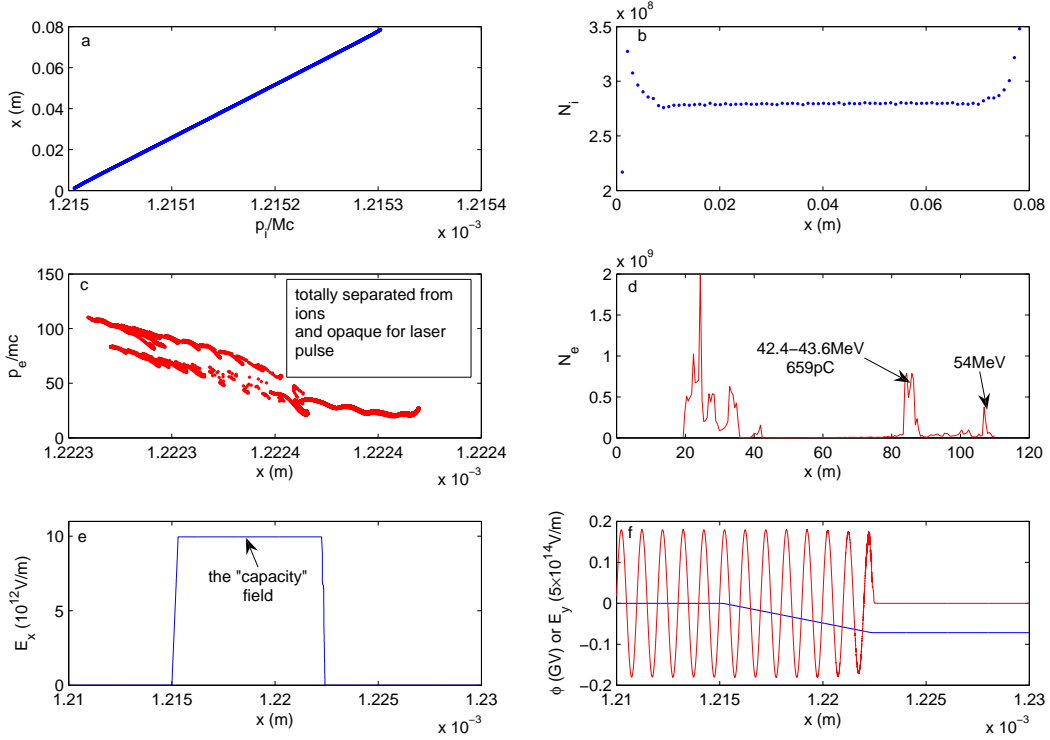


FIG. 1. (Color online) Simulation results by one-dimensional VORPAL at  $t = 25\text{fs}$ : the first opaque relativistic electron shell forms and is totally separated from ions. (a) and (c): the phase space distribution of ions and electrons. The electron shell is totally separated from the ions and is relativistic and opaque for laser pulse. (b) and (d): the density distribution of the ions and electrons with normalized momentum. The ion energy distribution is uniform. The electron energy distribution contains several monoenergetic ones. (e): the longitudinal space charge separation field, which is similar to the field in a capacity, is uniform and is  $9.95 \times 10^{12}\text{V/m}$ . (f): the potential and laser field. The electron shell is relativistic and opaque for the laser pulse.

as shown by Figure 2 (d). Figure 2 (f) shows that the deepness of the potential well for electrons increases about to  $0.3\text{GeV}$ . From Figure 2 (a) and (b), the maximum ion energy is about  $500\text{MeV}$ . The acceleration length is about  $65\mu\text{m}$ . A monoenergetic electron beam of  $186\text{MeV}$  and  $132\text{pC}$  is obtained as shown by Figure 2 (d). It is obvious that the first relativistic electron shell is still opaque for the laser pulse.

As shown by Figure 3 (d), the recirculating electrons cumulate and drive up the electron potential. In front of and behind the accumulating electrons, two potential wells are forming

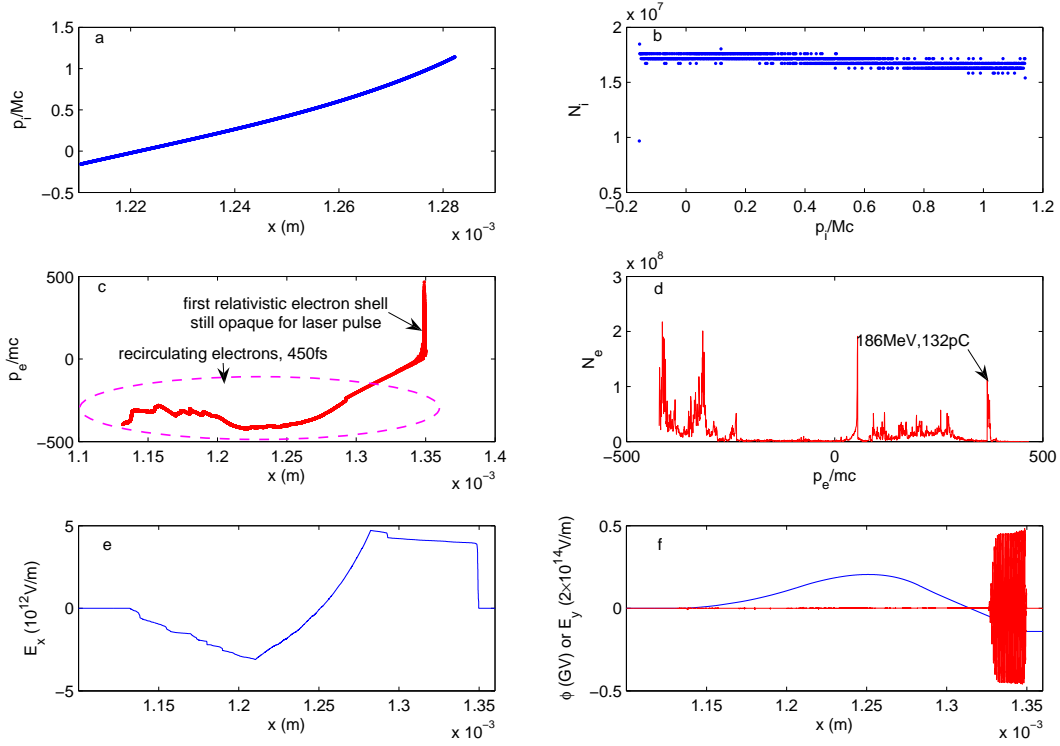


FIG. 2. (Color online) Simulation results by one-dimensional VORPAL at  $t = 450\text{fs}$ : electron recirculation begins and generates a potential well for electrons, where  $p_i, p_e$  is momentum of ion and electron respectively,  $M$  is the proton mass. (a) and (c): the phase space of ions and electrons respectively. The electron recirculation happens and some of them move in the opposite direction relativistically. (b) and (d): the energy distribution of ions and electrons respectively. The first electron shell is accelerated most efficiently and continuously. (e) the longitudinal field decreases due to the electron recirculation. However it is still uniform between the ion front and the first electron shell. (f): a potential hill for ions and a potential well for electrons forms due to the electron recirculation. The first relativistic electron shell maintains opaque for the laser pulse.

for electrons. The potential well I still traps and accelerates the accumulating electrons to generate the second relativistic high-density electron shell. In the potential well II, some electrons at the end of the second relativistic electron shell drop into it and will be trapped and accelerated to form a suprathermal electron shell as shown by Figure 5 (d). At the same time and at the local position of the second relativistic electron shell, potential well III for ions traps lots of ions and accelerates them to be relativistic and monoenergetic.

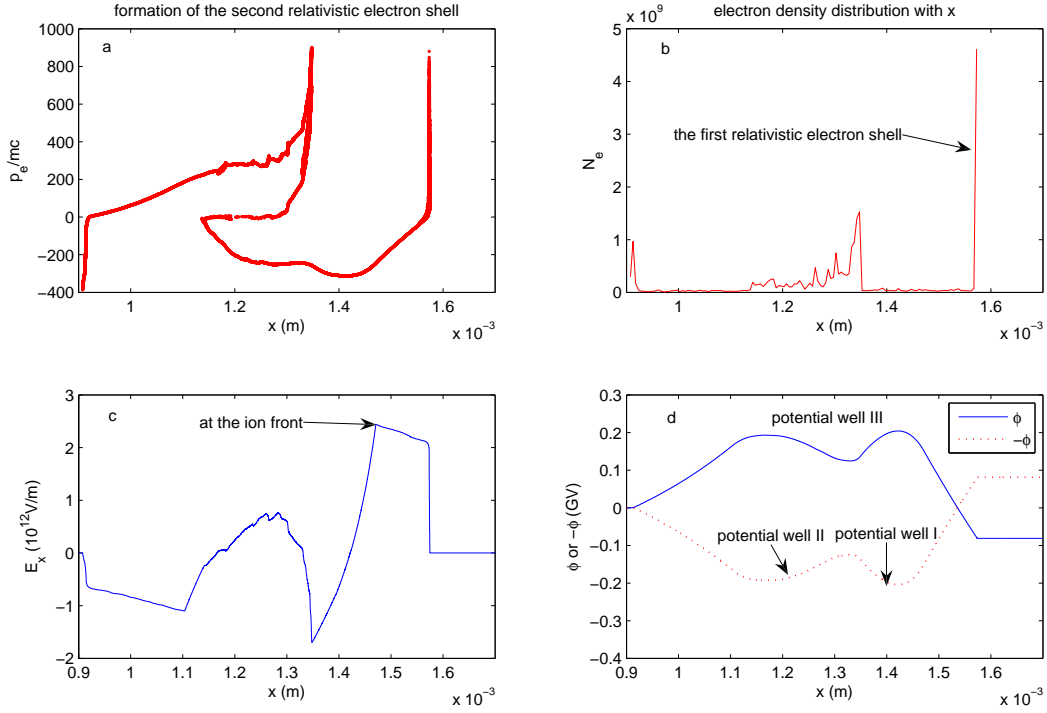


FIG. 3. (Color online) Simulation results by one-dimensional VORPAL at  $t = 1.25\text{ps}$ : the second relativistic electron shell forms and traps ions to be accelerated to relativistic. (a): the second relativistic electron shell forms in the potential well. It drives up the potential and forms two potential well I and II for electrons in front of and behind itself, a potential well III for ions at the local position of itself. It is shown clearly in (d). (b): the number density distribution of electrons. (c): the electron recirculation decreases the longitudinal field continuously. It is still uniform between the ion front and the first electron shell.

With time, the slow recirculating electrons can also be trapped in potential well V as shown in Figure 4(f) and the third suprathermal electron shell forms in the potential well II as shown by Figure 5. At the position of the shell, potential well IV traps the ions and accelerates them to obtain a quasi-monoenergetic distribution of  $171 \pm 10\text{MeV}$ . Behind the shell, a potential well for electrons traps them and a thermal electron cloud is generated. The ions between the double relativistic electron shell have a uniform distribution from  $1\text{GeV}$  to  $2.18\text{GeV}$ . Trapped by the second relativistic electron shell, the maximum energy reach  $981\text{MeV}$ . As shown in Figure 4 (f), the potential well III has been filled up nearly, then the energy dispersion will become worse. The ions with larger energy will coast down the

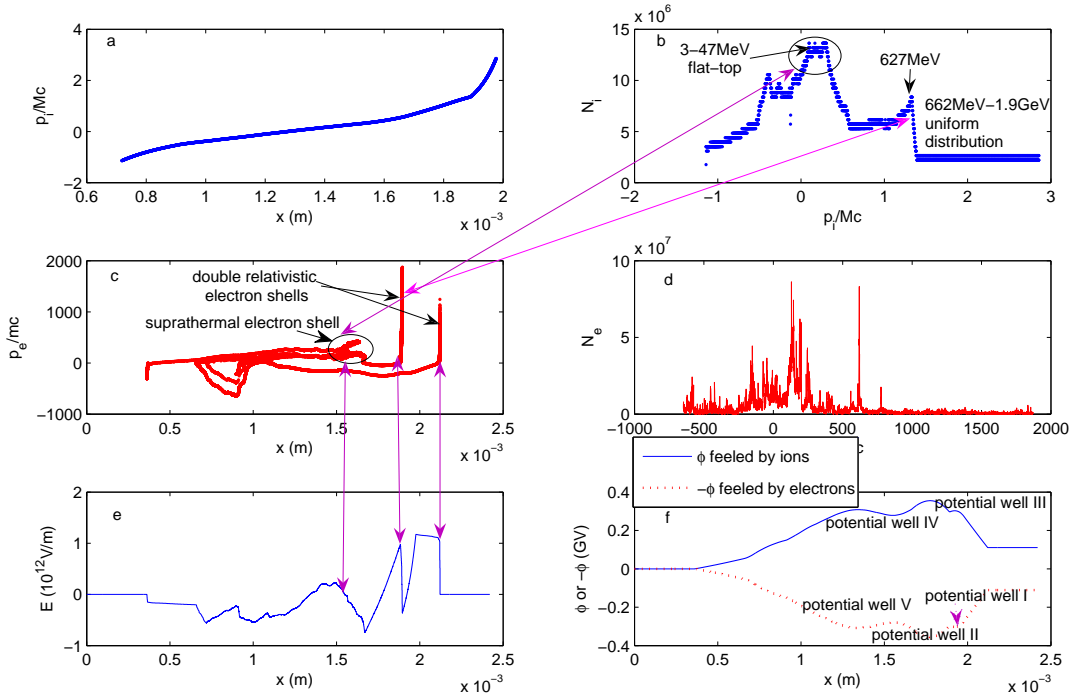


FIG. 4. (Color online) Simulation results by one-dimensional VORPAL at  $t = 3.075\text{ps}$ : the suprathermal electron shell forms and traps ions to obtain a flap-top 3 – 47MeV energy distribution. (a) and (c): the phase space of ions and electrons. The suprathermal electron shell forms in the potential well II and then potential V for electrons and potential IV are generated. (b) and (d) the energy distribution of ions and electrons. A monoenergy ion beam with energy of 627MeV is obtained in the second relativistic electron shell. (e): the longitudinal field induced by the double electron shell. (f): the potential IV for ions is induced by the suprathermal electron shell and traps ions and improves the energy dispersion of the 3 – 47MeV ion beam. The potential V can trap slow electrons and thermalize them to obtain thermal electron cloud. Potential III is nearly filled to be flat and the energy dispersion of the 627MeV monoenergetic ion beam will become worse.

following potential slope and get into the ion beam between the double relativistic electron shell. The ion number has a steep descent for the energy larger than 981MeV and has a slow drop for the energy smaller than 981MeV. In the electron energy distribution, there is a monoenergetic one of  $385 \pm 10\text{MeV}$  and 163pC, a ultra-relativistic one of 1GeV and a Maxwellian one which contains the thermal electron cloud and the suprathermal electron shell. As shown by Figure 5(c) and (f), the ion front is between the double electron shell. The

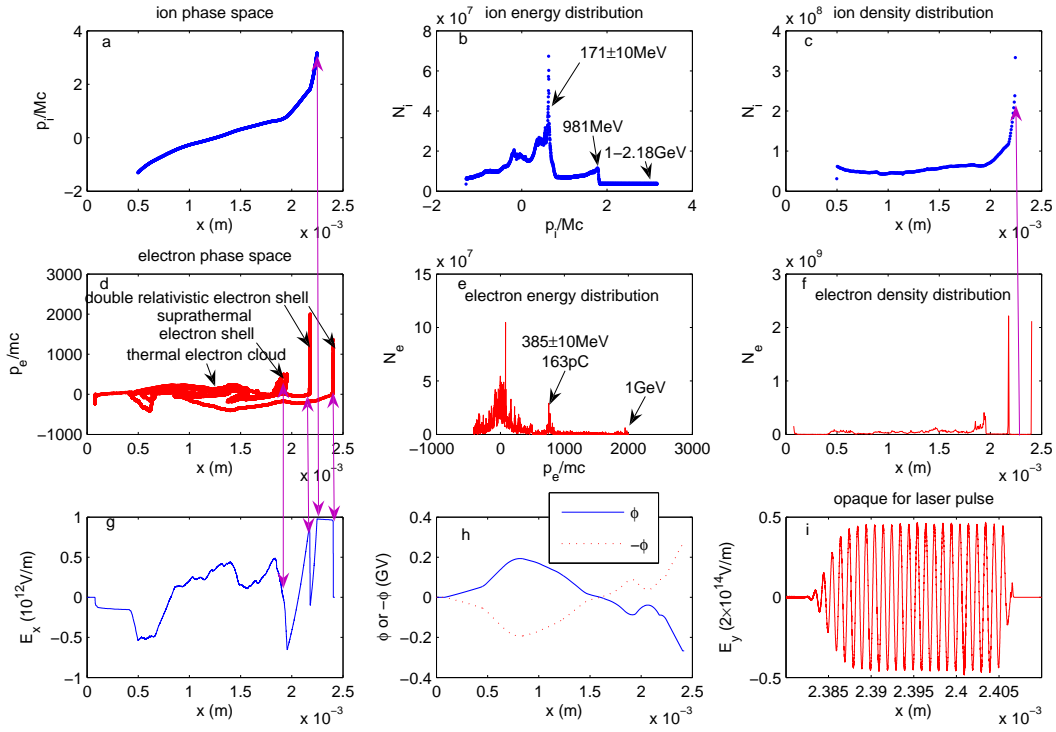


FIG. 5. (Color online) Simulation results by one-dimensional VORPAL at  $t = 4.025\text{ps}$ : the thermal electron cloud and the suprathermal electron shell come into being. (a) and (d): the phase-space of ions and electrons respectively. The electrons contain four main parts: the double relativistic electron shells, the suprathermal electron shell, the thermal electron cloud. (b) and (e): the energy distribution of ions and electrons respectively. A monoenergetic ion beam with energy of  $171 \pm 10\text{MeV}$  is obtained by the suprathermal electron shell. Trapped and accelerated by the second relativistic electron shell, the ion energy distribution drops down at  $981\text{MeV}$ . (c) and (f) the number density of ions and electrons respectively. (g) the longitudinal field. (h) the potential for ions and electrons. (i) the laser pulse field. The first electron shell maintains opaque for laser pulse.

ions between the double electron shell coast down the potential slope and obtain relativistic energy as shown in Figure 5(h) and (b).

In conclusion, the double relativistic electron shells, the suprathermal electron shell and the thermal electron cloud induce a new region of laser particle acceleration. In the process, several potential wells for ions and electrons are generated. On the whole, the double



relativistic electron shells induce two relativistic platforms of the ion energy distribution. The suprathermal electron shell traps and accelerates a monoenergetic ion beam with several hundreds of MeV, whose relative energy dispersion is near 5%. Together with the thermal electron cloud, a thermal Maxwellian ion beam has been obtained.

The authors would like to thank Dr. Hong-Yu Wang for useful discussion. The computation was carried out at the HSCC of Beijing Normal University. This work was supported by the Key Project of Chinese National Programs for Fundamental Research (973 Program) under contract No. 2011CB808104 and the Chinese National Natural Science Foundation under contract No. 10834008.

---

\* <http://www.anianet.com/adward>; [huangyongs@gmail.com](mailto:huangyongs@gmail.com)

- [1] F. Mako and T. Tajima, *Phys. Fluids* **27**, 1815 (1984).
- [2] H. Schwoerer, S. Pfotenhauer, O. Jackel, et al., *Nature* **439**, 445 (2006). *electronacc*
- [3] T. Esirkepov, M. Borghesi, S. V. Bulanov, G. Mourou, and T. Tajima, *Phys. Rev. Lett.* **92**, 175003 (2004).
- [4] A. Henig, S. Steinke, M. Schnrer, et al., *Phys. Rev. Lett.* **103**, 245003 (2009).
- [5] H. Schwoerer, S. Pfotenhauer, O. Jackel, et al., *Nature* **439**, 445 (2006).
- [6] X. Q. Yan, C. Lin, Z.M. Sheng, et al., *Phys. Rev. Lett.* **100**, 135003 (2008).
- [7] S. V. Bulanov, E. Yu. Echkina, T. Zh. Esirkepov, et al., *Phys. Rev. Lett.* **104**, 135003 (2010).
- [8] X. Q. Yan, T. Tajima, M. Hegelich, et al., *Appl. Phys. B*, 98711-721 (2010).
- [9] Y. S. Huang,
- [10] T. P. Yu, A. Pukhov, G. Shvets, and M. Chen, *Phys. Rev. Lett.* **105**, 065002 (2010).
- [11] A. Macchi, F. Cattani, T. V. Liseykina and F. Cornolti, *Phys. Rev. Lett.* **94**, 165003 (2005).